SRFormerV2: Taking a Closer Look at Permuted Self-Attention for Image Super-Resolution

Yupeng Zhou, Zhen Li, Chun-Le Guo, Li Liu, Senior Member, IEEE, Ming-Ming Cheng, Senior Member, IEEE, Qibin Hou, Member, IEEE

Abstract—Previous works have shown that increasing the window size for Transformer-based image super-resolution models (e.g., SwinIR) can significantly improve the model performance. Still, the computation overhead is also considerable when the window size gradually increases. In this paper, we present SRFormer, a simple but novel method that can enjoy the benefit of large window self-attention but introduces even less computational burden. The core of our SRFormer is the permuted self-attention (PSA), which strikes an appropriate balance between the channel and spatial information for self-attention. Without any bells and whistles, we show that our SRFormer achieves a 33.86dB PSNR score on the Urban100 dataset, which is 0.46dB higher than that of SwinIR but uses fewer parameters and computations. In addition, we also attempt to scale up the model by further enlarging the window size and channel numbers to explore the potential of Transformer-based models. Experiments show that our scaled model, named SRFormerV2, can further improve the results and achieves state-of-the-art. We hope our simple and effective approach could be useful for future research in super-resolution model design. The homepage is https://z-yupeng.github.io/SRFormer/.

Index Terms—Super-resolution, vision transformer, permuted self-attention, window size

1 Introduction

SINGLE image super-resolution (SR) aims to restore a high-quality image from its degraded low-resolution version. Exploring efficient and effective super-resolution algorithms has been a hot research topic in computer vision, which has a variety of applications [2], [3], [4]. Since the pioneer works [5], [6], [7], [8], [9], [10], CNN-based methods have been mainstream for image super-resolution for a long time. These methods mostly take advantage of residual learning [11], [8], [10], [6], [12], [13], dense connections [14], [15], [16], or channel attention [17], [18] to construct network architectures, making great contributions to the development of super-resolution models.

Despite the success made by CNN-based models in super-resolution, recent works [19], [20], [21], [22] have shown that Transformer-based models perform better. They observe that self-attention, which can build pairwise relationships, is a more efficient way to produce high-quality super-resolution images than convolutions. One typical work among them should be SwinIR [20], which introduces Swin Transformer [23] to image super-resolution, greatly improving the CNN-based models on various benchmarks. Later, a variety of works, such as SwinFIR [21], ELAN [22], and HAT [24], further develop SwinIR and use Transformers to design different network architectures for SR.

The methods above reveal that properly enlarging the windows for the shifted window self-attention in SwinIR can result in clear performance gain (see Fig. 1). However, the computational burden is also an important issue as the

Manuscript received March 1, 2022; revised August 26, 2022.

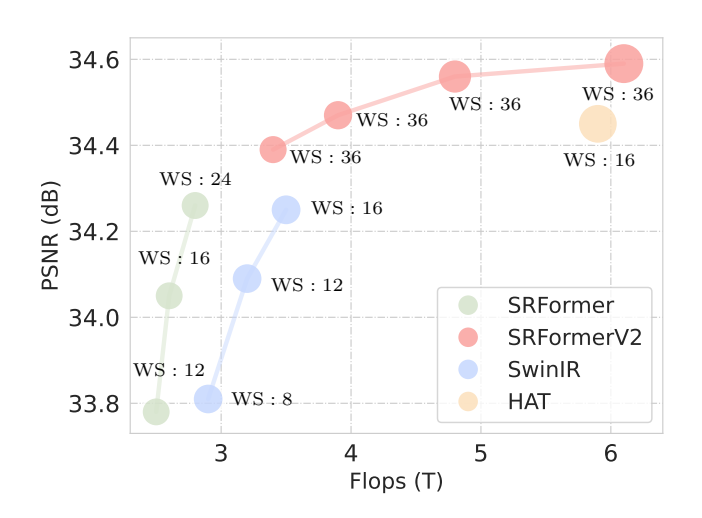


Fig. 1. Performance comparison among SwinIR, HAT, our SRFormer and SRFormerV2. The radius of the circles represents the parameters of the models. "WS" stands for the attention window size, e.g. "WS: 24 " stands for 24×24 attention windows. Our SRFormer enjoys large window sizes with even fewer computations but higher PSNR scores.

window size becomes larger. In addition, Transformer-based methods utilize self-attention and require networks of larger channel numbers than previous CNN-based methods [17], [15], [6]. To explore efficient and effective super-resolution algorithms, a straightforward question should be: How would the performance go if we reduce the channel number and increase the window size?

Motivated by the above question, in our conference version of this work [1], we present permuted self-attention (PSA), an efficient way to build pairwise relationships within large windows (e.g., 24×24). The intention is to en-

Y. Zhou, Z. Li, C.L. Guo, M.M. Cheng, and Q. Hou are with VCIP, CS, Nankai University, Tianjin, China.

L. Liu is with NUDT, Changsha, China.

[•] Q. Hou is the corresponding author.

[•] The previous version of this paper has been accepted by ICCV 2023 [1].

able more pixels to participate in the attention map computation while introducing no extra computational burden. To this end, we propose to shrink the channel dimensions of the key and value matrices and adopt a permutation operation to convey part of the spatial information into the channel dimension. In this way, despite the channel reduction, there is no loss of spatial information, and each attention head is also allowed to keep a proper number of channels to produce expressive attention maps [25]. In addition, we also improve the original feed-forward network (FFN) by adding a depth-wise convolution between the two linear layers, which we found helps in high-frequency component recovery.

Given the proposed PSA, we construct a novel network for SR in the conference version, termed SRFormer. Benefiting from the proposed PSA, our SRFormer receives good performance on five widely-used datasets. Notably, for $\times 2$ SR, our SRFormer trained on only the DIV2K dataset [10] achieves a 33.86 PSNR score on the challenging Urban100 dataset [26]. This result is much higher than the popular SwinIR (33.40) and ELAN (33.44). A similar phenomenon can be observed when evaluating the $\times 3$ and $\times 4$ SR tasks. In addition, we perform experiments using a light version of our SRFormer. Our method performs better on all benchmarks than previous lightweight SR models.

Despite the good performance of our SRFormer, the scaling ability of SRFormer has not been explored well. In this paper, we intend to further investigate the scaling ability of SRFormer and conduct a series of scaling operations. To our knowledge, due to PSA's efficient computation of window attention, we are the first to implement self-attention computation within 40×40 windows. Experimental results demonstrate that conducting attention calculations within larger windows can further improve performance, showing our method's excellent scaling capabilities. By conducting a series of scaling operations, our new model, named SRFormerV2, is able to surpass the state-of-the-art HAT method [24] with less computational cost and parameters. To sum up, the contributions of this paper can be summarized as follows:

- We propose a novel permuted self-attention mechanism for image super-resolution, which can enjoy large-window self-attention by transferring spatial information into the channel dimension. By leveraging it, we are able to implement the self-attention mechanism within 40 × 40 windows at an acceptable time complexity for SR.
- We build a new transformer-based super-resolution network, dubbed SRFormer, based on the proposed PSA and an improved FFN from the frequency perspective (ConvFFN).
- Based on SRFormer, we further explore the scaling capability of the model at the macro structural level and consider the use of both large and small window PSA. The outcome of the above investigations is the new SRFormerV2, which is able to surpass previous state-of-the-art models using fewer parameters and computational cost.

2 RELATED WORK

In this section, we briefly review the literature on image super-resolution. We first introduce the CNN-based methods and then describe the recently popular Transformer-based models.

2.1 CNN-Based Image Super-Resolution

Since SRCNN[5] first introduced CNN into image superresolution (SR), many CNN-based SR models have emerged. DRCN [27] and DRRN [11] introduce recursive convolutional networks to increase the depth of the network without increasing the parameters. Some early CNN-based methods [28], [5], [27], [11] attempt to interpolate the lowresolution (LR) as input, which results in a computationally expensive feature extraction. To accelerate the SR inference process, FSRCNN [29] extracts features at the LR scale and conducts an upsampling operation at the end of the network. This pipeline with pixel shuffle upsampling [9] has been widely used in later works [22], [17], [20]. LapSRN [30] and DBPN [31] perform upsampling during extracting features to learn the correlation between LR and HR. There are also some works [8], [14], [32], [33] that use GAN [34] to generate realistic textures in reconstruction. MemNet [28], RDN [15], and HAN [35] efficiently aggregate the intermediate features to enhance the quality of the reconstructed images. Non-local attention [36] has also been extensively explored in SR to better model the long-range dependencies. Methods of this type include CS-NL [37], NLSA [38], SAN [39], IGNN [40], etc.

2.2 Vision Transformers

Transformers have recently shown great potential in a variety of vision tasks, including image classification [41], [42], [43], [44], [45], object detection [46], [47], [48], semantic segmentation [49], [50], [51], image restoration [52], [20], [19], etc. Among these, the most typical work should be Vision Transformer (ViT) [41], which proves Transformers can perform better than convolutional neural networks on feature encoding. The application of Transformers in low-level vision mainly includes two categories: generation [53], [54], [55], [56] and restoration. Further, the restoration tasks can also be divided into two categories: video restoration [57], [58], [59], [60], [61] and image restoration [19], [52], [62], [63].

Image super-resolution is an important task in image restoration. It needs to preserve the structural information of the input, which is a great challenge for Transformer-based model design. IPT [19] is a large pre-trained model based on the Transformer encoder and decoder structure and has been applied to super-resolution, denoising, and deraining. Based on the Swin Transformer encoder [23], SwinIR [20] performs self-attention on an 8×8 local window in feature extraction and achieves extremely powerful performance. ELAN [22] simplifies the architecture of SwinIR and uses self-attention computed in different window sizes to collect the correlations between long-range pixels.

Our SRFormer is also based on Transformer. Unlike the methods above that directly leverage self-attention to build models, our SRFormer mainly aims at the self-attention

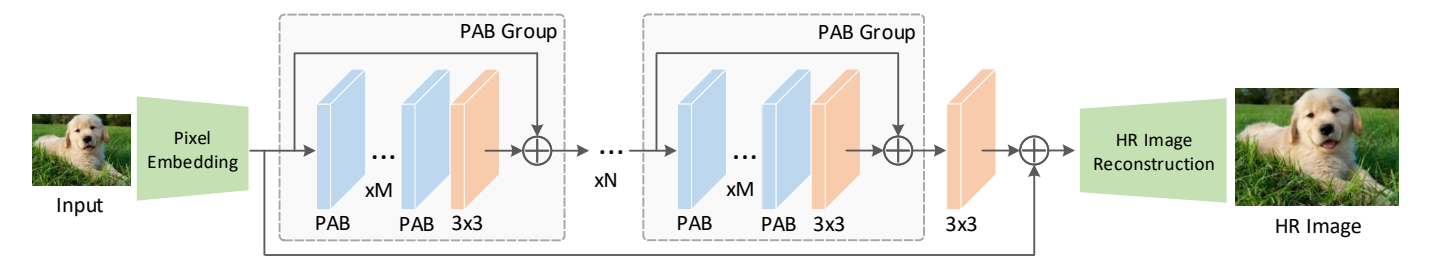


Fig. 2. Overall architecture of SRFormer. The pixel embedding module is a 3×3 convolution to map the input image to feature space. The HR image reconstruction module contains a 3×3 convolution and a pixel shuffle operation to reconstruct the high-resolution image. The middle feature encoding part has N PAB groups, followed by a 3×3 convolution.

itself. We intend to study how to compute self-attention in a large window to improve the performance of SR models without increasing the parameters and computational cost.

3 METHOD

3.1 Overall Architecture

The overall architecture of our SRFormer and SRFormerV2 is shown in Fig. 2, consisting of three parts: a pixel embedding layer G_P , a feature encoder G_E , and a highresolution image reconstruction layer G_R . Following previous works [20], [22], the pixel embedding layer G_P is a single 3×3 convolution that transforms the low-resolution RGB image $I \in \mathbb{R}^{H\times W\times 3}$ to feature embeddings $F_P \in \mathbb{R}^{H\times W\times C}$. F_P will then be sent into the feature encoder G_E with a hierarchical structure. It consists of N permuted selfattention groups, each of which is with M permuted selfattention blocks followed by a 3×3 convolution. A 3×3 convolution is added at the end of the feature encoder, yielding F_E . The summation results of F_E and F_P are fed into G_R for high-resolution image reconstruction, which contains a 3×3 convolution and a sub-pixel convolutional layer [9] to reconstruct high-resolution images. We compute the L1 loss between the high-resolution reconstructed image and ground-truth HR image to optimize our models.

3.2 Permuted Self-Attention Block

The core of our SRFormer and SRFormerV2 is the permuted self-attention block (PAB), which consists of a permuted self-attention (PSA) layer and a convolutional feed-forward network (ConvFFN).

Permuted self-attention. As shown in Fig. 3(b), given an input feature map $\mathbf{X}_{in} \in \mathbb{R}^{H \times W \times C}$ and a tokens reduction factor r, we first split \mathbf{X}_{in} into N non-overlapping square windows $\mathbf{X} \in \mathbb{R}^{NS^2 \times C}$, where S is the side length of each window. Then, we use three linear layers L_Q, L_K, L_V to get \mathbf{Q} , \mathbf{K} , and \mathbf{V} :

$$\mathbf{Q}, \mathbf{K}, \mathbf{V} = L_Q(\mathbf{X}), L_K(\mathbf{X}), L_V(\mathbf{X}). \tag{1}$$

Here, \mathbf{Q} keeps the same channel dimension to \mathbf{X} while L_K and L_V compress the channel dimension to C/r^2 , yielding $\mathbf{K} \in \mathbb{R}^{NS^2 \times C/r^2}$ and $\mathbf{V} \in \mathbb{R}^{NS^2 \times C/r^2}$. After that, to enable more tokens to get involved in the self-attention calculation and avoid the increase of the computational cost, we propose to permute the spatial tokens in \mathbf{K} and \mathbf{V} to the channel dimension, attaining permuted tokens $\mathbf{K}_p \in \mathbb{R}^{NS^2/r^2 \times C}$ and $\mathbf{V}_p \in \mathbb{R}^{NS^2/r^2 \times C}$.

We use \mathbf{Q} and the shrunken \mathbf{K}_p and \mathbf{V}_p to perform the self-attention operation. In this way, the window size for \mathbf{K}_p and \mathbf{V}_p will be reduced to $\frac{S}{r} \times \frac{S}{r}$ but their channel dimension is still unchanged to guarantee the expressiveness of the attention map generated by each attention head [25]. The formulation of the proposed PSA can be written as follows:

$$PSA(\mathbf{Q}, \mathbf{K}_p, \mathbf{V}_p) = Softmax \left(\frac{\mathbf{Q} \mathbf{K}_p^T}{\sqrt{d_k}} + \mathbf{B} \right) \mathbf{V}_p, \quad (2)$$

where B is an aligned relative position embedding that can be attained by interpolating the original one defined in [23] since the window size of Q does not match that of \mathbf{K}_{p} . $\sqrt{d_{k}}$ is a scalar as defined in [41]. Note that the above equation can easily be converted to the multi-head version by splitting the channels into multiple groups. Our PSA transfers the spatial information to the channel dimension. It ensures the following two key design principles: i) We do not downsample the tokens first as done in [49], [44] but allow each token to participate in the self-attention computation independently. This enables more representative attention maps. We will discuss more variants of our PSA in Sec. 3.3 and show more results in our experiment section. ii) In contrast to the original self-attention illustrated in Fig. 3(a), PSA can be conducted in a large window (e.g., 24×24) using even fewer computations than SwinIR with 8×8 window while attaining better performance.

ConvFFN. Previous works have demonstrated that selfattention can be viewed as a low-pass filter [64], [65]. To better restore high-frequency information, a 3 × 3 convolution is often added at the end of each group of Transformers as done in SwinIR [20]. Different from SwinIR, in our PAB, we propose to add a local depthwise convolution branch between the two linear layers of the FFN block to assist in encoding more details. We name the new block ConvFFN. We empirically found that such an operation increases nearly no computations but can compensate for the loss of high-frequency information caused by self-attention shown in Fig. 4. We simply calculate the power spectrum of the feature maps produced by our SRFormer with FFN and ConvFFN. By comparing the two figures, we can see that ConvFFN can clearly increase high-frequency information, and hence yields better results as listed in Tab. 1.

3.3 Large-Window Self-Attention Variants

To provide guidance for the design of large-window selfattention and demonstrate the advantage of our PSA, here,

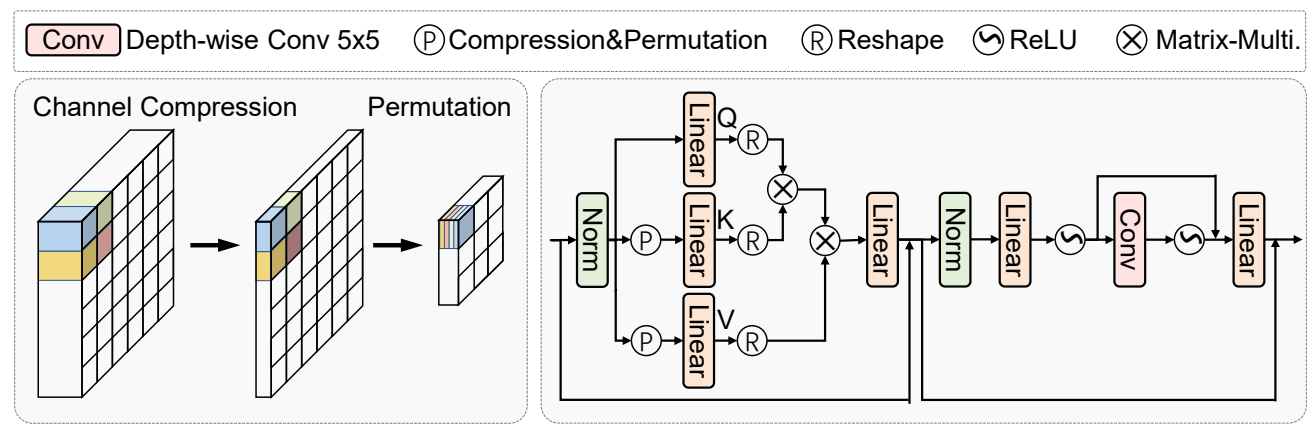


Fig. 3. Comparison between (a) self-attention and (b) our proposed permuted self-attention. To avoid spatial information loss, we propose to reduce the channel numbers and transfer the spatial information to the channel dimension.

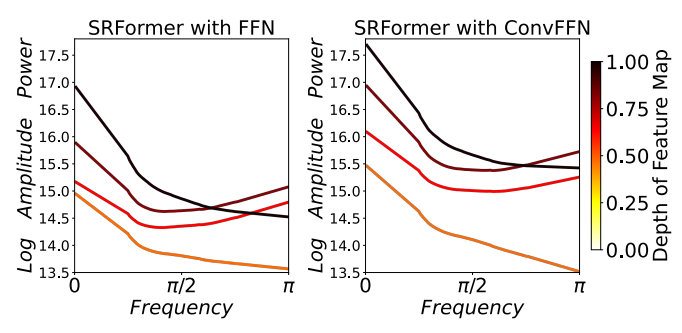


Fig. 4. Power spectrum of the intermediate feature maps produced by our SRFormer with FFN and ConvFFN. Lines in darker color correspond to features from deeper layers.

we introduce another two large-window self-attention variants. The quantitative comparisons and analysis can be found in our experiment section.

Token Reduction. The first way to introduce large-window self-attention and avoid the increase in computational cost is to reduce the number of tokens as done in [49]. Let r and S be a reduction factor and the window size. Given an input $\mathbf{X} \in \mathbb{R}^{N \times S^2 \times C}$, we can adopt a depthwise convolutional function with kernel size $r \times r$ and stride r to reduce the token numbers of \mathbf{K} and \mathbf{V} in each window to $(\frac{S}{r})^2$, yielding $\mathbf{Q}_r \in \mathbb{R}^{N \times S^2 \times C}$, $\mathbf{K}_r \in \mathbb{R}^{N \times S^2/r^2 \times C}$, and $\mathbf{V}_r \in \mathbb{R}^{N \times S^2/r^2 \times C}$. \mathbf{Q}_r and \mathbf{K}_r are used to compute the attention scores $\mathbf{A} \in \mathbb{R}^{N \times S^2 \times S^2/r^2}$. Computing the matrix multiplication between \mathbf{A} and \mathbf{V}_r yields the output with the same number of tokens to \mathbf{X} .

Token Sampling. The second way to achieve large-window self-attention is to randomly sample T^2 $(0 \le T \le S)$ tokens from each window according to a given sampling ratio t for the key \mathbf{K} and value \mathbf{V} . Given the input $\mathbf{X} \in \mathbb{R}^{NS^2 \times C}$, \mathbf{Q} shares the same shape with \mathbf{X} but the shapes of \mathbf{K} and \mathbf{V} are reduced to $NT^2 \times C$. In this way, as long as T is fixed, the computational cost increases linearly as the window size gets larger. A drawback of token sampling is that randomly selecting a portion of tokens loses structural information of the scene content, which is essentially needed for image super-resolution. We will show more numerical results in our experiment section.

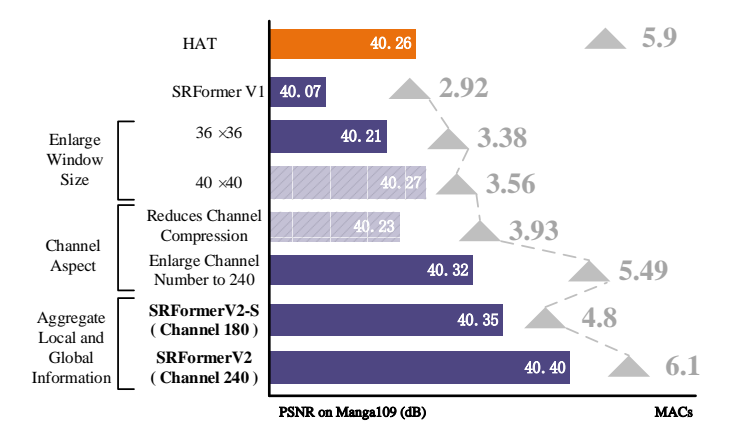


Fig. 5. The enhancement roadmap for SRFormerV2 begins with the original SRFormer. Through multifaceted improvements, we scale our SRFormer up and achieve significant performance enhancements. The backslash block indicates enhancement methods can also improve performance but are not adopted in SRFormerV2. The orange square represents the previous state-of-the-art (SOTA) methods, HAT [24].

4 SRFORMERV2: SCALING THE SRFORMER

In this section, we further explore the potential of our SR-Former by scaling it up as shown in Fig. 5 and present a new version, SRFormerV2. We intend to figure out two things: i) Whether PSA with a larger window can further boost the performance; ii) How to balance the channel and spatial information, as well as the local and global information to maximize the effect of PSA.

Scaling the window size. The original SRFormer employs permuted self-attention to perform SR reconstruction efficiently. By compressing the channel information and transferring spatial information, PSA can enjoy large-window self-attention with fewer computations, boosting the performance of previous Transformer-based models. Leveraging the PSA, we can enjoy large window self-attention with acceptable computations. Thus, it is natural to investigate whether larger windows could further lift the performance.

To figure it out, we conduct more experiments to further enlarge the window size, as shown in Tab. 4. We find that for the low-resolution test set, such as Set5 or B100, the performance no longer improves when we scale the window size up to 36×36 . However, we find that in high-

resolution test datasets, such as Urban100 or Manga109, even when we reach the maximum level allowed by our computational resources, a window size of 40×40 , notable improvements in performance can still be achieved. This finding provides strong evidence for the significance of larger attention windows in image super-resolution, which is inspiring for super-resolution backbone design. It is worth noting that, by leveraging PSA, our computations are still reasonable even with the 40×40 window size, more efficient and effective than the recent state-of-the-art model HAT. In the end, we set the window size of 36×36 to strike a balance between computational cost and performance.

Another advantage we discover when increasing the window size is the superiority of the structural similarity index measure (SSIM). As shown in Tab. 5, our SRFormer almost always achieves the highest SSIM values, even in cases where our Peak Signal-to-Noise Ratio (PSNR) values are similar to those of the comparison models. SSIM [66] is proposed to measure the differences between the structure properties of the areas. Instead of simply computing the absolute error between the images like PSNR, SSIM is proposed to take into account known properties of the human visual system.

Scaling in the channel aspect. Another scaling exploration is to enlarge the channel number. The original PSA compresses the channel number, so there is some sacrifice in channel information. By scaling the channel number, we hope to compensate for the loss of channel information. As shown in the channel aspect bracket of Fig. 5, two explorations are carried out: i) We enlarge the channel number to preserve more channel information. Increasing the number of channels allows the use of more information during inference, which results in significant performance gains. However, it also leads to an increase in computational load. By integrating the operations of scaling the channel size and the scaling window size mentioned earlier, we can achieve significant improvements compared to the original results of SRFormer. ii) Reduce the degree of channel compression. Our permuted self-attention compresses the channel dimension and transfers the spatial information to the channel dimension. By increasing the number of channels after compression, we can reduce the loss of channel information. This brings some improvements, but it is not adopted in SRFormerV2 after taking account of the performance improvement and computing overhead.

Aggregating Global and Local information. Based on PSA, we are able to facilitate a broad range of information interchange with a very small computational cost. However, as shown in [67], the local information also plays a significant role in enhancing the performance of SR. During the expiration, we hope to introduce the local spatial information into our large window self-attention SR network. We rethink the macro architecture of the network and attempt to involve more local information. Following previous SR models [20], the size of attention windows in SRFormer is all the same. However, due to the advantage of our PSA, our attention window size is particularly large, as it is conducive to aggregating global information. In order to further improve performance, we contemplate whether we could also introduce some blocks with small attention windows to help

capture local information. Therefore, prior to every two permute self-attention blocks (abbreviated as PAB shown in Fig. 2), we insert a block with a small window size, to aggregate local spatial information before gathering global information. We found that such an approach is particularly useful for enhancing performance.

By combining the aforementioned enhancement methods as shown in Fig. 5, we have upgraded SRFormer to SRFormerV2, achieving a new state-of-the-art. With a similar computational cost, it largely improves the previous state-of-the-art HAT. We name the scaling version as SRFormerV2. We also design a version with even less computational cost named SRFormerV2-S, which still achieves comparable performance with HAT.

5 EXPERIMENTS

In this section, we conduct experiments on both the classical, lightweight, and real-world image SR tasks, compare our SRFormer and SRFormerV2 with existing state-of-the-art methods, and do ablation analysis of the proposed method.

5.1 Experimental Setup

Datasets and Evaluation. The choice of training datasets remains the same as the comparison models. In classical image SR, we use DIV2K [10] and DF2K (DIV2K [10] + Flickr2K [72]) to train two versions of SRFormer. In the training of SRFormerV2, we also use DF2K as the training dataset. For lightweight image SR, we use DIV2K [10] to train our SRFormer-light. For real-world SR, we use DF2K and OST [73]. For testing, we mainly evaluate our method on five benchmark datasets, including Set5 [68], Set14 [69], BSD100 [70], Urban100 [26], and Manga109 [71]. Self-ensemble strategy is introduced in SRFormerV2 to further improve performance, marked as SRFormerV2+. The experimental results are evaluated in terms of PSNR and SSIM values, which are calculated on the Y channel from the YCbCr space.

Implementation Details. In the classical image SR task, we set the PAB group number, PAB number, channel number, and attention head number to 6, 6, 180, and 6, respectively. When training SRFormer on DIV2K [10], the patch size, window size S, and reduction factor r are set to 48×48 , 24, and 2, respectively. When training SRFormer on the DF2K [10], [72], they are 64×64 , 22, and 2, respectively. For the training of SRFormerV2, we also follow the same training settings. For the lightweight image SR task, we set the PAB group number, PAB number, channel number, windows size S, reduction factor r, and attention head number to 4, 6, 60, 16, 2, and 6, respectively. The training patch size we use is 64×64 . We randomly rotate images by 90° , 180° , or 270° and randomly flip images horizontally for data augmentation. We adopt the Adam [74] optimizer with $\beta_1 = 0.9$ and $\beta_2 = 0.99$ to train the model for 500k iterations. The initial learning rate is set as 2×10^{-4} and is reduced by half at the $\{250k, 400k, 450k, 475k\}$ -th iterations.

5.2 Ablation Study

Impact of window size in PSA. Permuted self-attention provides an efficient and effective way to enlarge window

TABLE 1 Ablation study on the window size. We report results on the original SwinIR, SRFormer without ConvFFN, and our full SRFormer. Note that the parameters and MACs of SRFormer with 24×24 window are fewer than SwinIR with 8×8 window. Larger windows can result in better performance.

Method	Window size Params		Params MACs		SET5 [68]		SET14 [69]		B100 [70]		Urban100 [26]		Manga109 [71]	
				PSNR	SSIM	PSNR	SSIM	PSNR	SSIM	PSNR	SSIM	PSNR	SSIM	
SwinIR [20]	8×8	11.75M	2868G	38.24	0.9615	33.94	0.9212	32.39	0.9023	33.09	0.9373	39.34	0.9784	
	12×12	11.82M	3107G	38.30	0.9617	34.04	0.9220	32.42	0.9026	33.28	0.9381	39.44	0.9788	
	16×16	11.91M	3441G	38.32	0.9618	34.00	0.9212	32.44	0.9030	33.40	0.9394	39.53	0.9791	
SRFormer w/o ConvFFN	12×12	9.97M	2381G	38.23	0.9615	34.00	0.9216	32.37	0.9023	32.99	0.9367	39.30	0.9786	
	16×16	9.99M	2465G	38.25	0.9616	33.98	0.9209	32.38	0.9022	33.09	0.9371	39.42	0.9789	
	24×24	10.06M	2703G	38.30	0.9618	34.08	0.9225	32.43	0.9030	33.38	0.9397	39.44	0.9786	
SRFormer	12×12	10.31M	2419G	38.22	0.9614	34.08	0.9220	32.38	0.9025	33.08	0.9372	39.13	0.9780	
	16×16	10.33M	2502G	38.31	0.9617	34.10	0.9217	32.43	0.9026	33.26	0.9385	39.36	0.9785	
	24×24	10.40M	2741G	38.33	0.9618	34.13	0.9228	32.44	0.9030	33.51	0.9405	39.49	0.9788	

TABLE 2 Ablation study on ConvFFN for $\times 2$ SR. From the results on Urban100 and Manga109, we can see that using 5×5 depthwise convolution yields the best results. This indicates that local details are also essential for Transformer-based models.

ConvFFN	Urban1	00 [26]	Manga109 [71]			
	PSNR	SSIM	PSNR	SSIM		
w/o Depth-wise Conv 3×3 Depth-wise Conv 5×5 Depth-wise Conv	33.38 33.42 33.51	0.9397 0.9398 0.9405	39.44 39.34 39.49	0.9786 0.9787 0.9788		

TABLE 3

imes 2 SR performance comparison among SwinIR [20], our proposed PSA, and the two variants on Urban100 [26]. The results reported here are based on the best model trained on DIV2K for 200k iterations. r and S are the reduction factor and the window size. For token sampling, r=S/T. PSA performs better than the other two variants.

Method	Params	MACs	S	r	PSNR	SSIM
SwinIR [20]	11.75M	2868G	8	-	33.09	0.9373
Token Reduction	11,78M	2471G	16	2 2	33.09	0.9372
Token Reduction	11.85M	2709G	24		33.24	0.9387
Token Sampling	11.91M	2465G	16	2	32.38	0.9312
Token Sampling	12.18M	2703G	24		32.34	0.9305
PSA	9.99M	2465G	16	2	33.09	0.9371
PSA	9.67M	2390G	24	3	33.09	0.9376
PSA	10.06M	2703G	24	2	33.38	0.9397

TABLE 4

We further scale the window size of SRFormer to explore our SRFormerV2. We report PSNR on Set5, B100, Urban100, and Manga109. All models are trained on the DF2K (DIV2K [10] + Flickr2K [72]) training set for 500k training iterators.

Window Size	MACs	Set5	B100	Urban100	Manga109
24×24	2741G	38.53	32.59	34.09	40.07
36×36	3377G	38.58	32.61	34.39	40.21
40×40	3562G	38.58	32.61	34.52	40.27

size. To investigate the impact of different window sizes on model performance, we conduct three groups of experiments and report the results in Table 1. The first group is the vanilla SwinIR [20] with 8×8 , 12×12 , and 16×16 window sizes. In the second group, we do not use the ConvFFN but only the PSA in our SRFormer and set the window size to 12×12 , 16×16 , and 24×24 , respectively, to observe the

performance difference. In the third group, we use our full SRFormer with $12\times12,\,16\times16,$ and 24×24 as window size to explore the performance change. The results show that a larger window size yields better performance improvement for all three groups of experiments. In addition, the parameters and MACs of our SRFormer with 24×24 window are even fewer than the original SwinIR with 8×8 window. To balance the performance and MACs, we set window size as 24×24 in SRFormer and 16×16 in SRFormer-light.

Impact of kernel size of ConvFFN. We introduce ConvFFN in Sec. 3.2, which aims to encode more local information without increasing too many computations. In order to explore which kernel size can bring the best performance improvement, we attempt to use 3×3 depth-wise convolution and 5×5 depth-wise convolution and report the results in Table 2. Given that the depth-wise convolution has little effect on the number of parameters and MACs, we do not list them in the table. Obviously, 5×5 depth-wise convolution leads to the best results. Thus, we use 5×5 depth-wise convolution in our ConvFFN.

Large-window self-attention variants. In Sec. 3.3, we introduce another two large-window self-attention variants. We summarize the results in Table 3. Though token reduction can slightly improve SwinIR when using a large window, the number of parameters does not decrease and the performance gain is lower than ours. We argue that it is because directly applying downsampling operations to the key and value results in spatial information loss. For token sampling, the performance is even worse than the original SwinIR. We believe the reason is that dropping out some tokens severely breaks the image content structure.

Further scaling window size in SRFormerV2. Here, we further explore the performance of SRFormer with larger attention windows in Sec. 4. Building upon a baseline of 24×24 , we implement attention mechanisms for window sizes of 36×36 and 40×40 , respectively. As shown in Tab. 4, for the largest window size we could achieve (40×40) , we still observe performance improvement. For low-resolution images, increasing the window size up to 36 results in similar performance. However, when further increasing the window size to 40×40 , we observe no performance gain due to the small input size.

TABLE 5

Quantitative comparison of our SRFormer with recent state-of-the-art classical image SR methods on five benchmark datasets. The best performance is highlighted.

	Method	Training	SET	5 [68]	SET1	4 [69]	B100	70]	Urban	100 [26]	Manga	109 [71]
	Wethou	Dataset	PSNR	SSIM	PSNR	SSIM	PSNR	SSIM	PSNR	SSIM	PSNR	SSIM
	EDSR [10]	DIV2K	38.11	0.9602	33.92	0.9195	32.32	0.9013	32.93	0.9351	39.10	0.9773
	RCAN [17]	DIV2K	38.27	0.9614	34.12	0.9216	32.41	0.9027	33.34	0.9384	39.44	0.9786
	SAN [39]	DIV2K	38.31	0.9620	34.07	0.9213	32.42	0.9028	33.10	0.9370	39.32	0.9792
	IGNN [40]	DIV2K	38.24	0.9613	34.07	0.9217	32.41	0.9025	33.23	0.9383	39.35	0.9786
SR	HAN [35]	DIV2K	38.27	0.9614	34.16	0.9217	32.41	0.9027	33.35	0.9385	39.46	0.9785
$\times 2$	NLSA [38]	DIV2K	38.34	0.9618	34.08	0.9231	32.43	0.9027	33.42	0.9394	39.59	0.9789
×	SwinIR [20]	DIV2K	38.35	0.9620	34.14	0.9227	32.44	0.9030	33.40	0.9393	39.60	0.9792
	ELAN [22]	DIV2K	38.36	0.9620	34.20	0.9228	32.45	0.9030	33.44	0.9391	39.62	0.9793
	SRFormer (ours)	DIV2K	38.45	0.9622	34.21	0.9236	32.51	0.9038	33.86	0.9426	39.69	0.9786
	IPT [19]	ImageNet	38.37	-	34.43	-	32.48	-	33.76	-	-	-
	SwinIR [20]	DF2K	38.42	0.9623	34.46	0.9250	32.53	0.9041	33.81	0.9427	39.92	0.9797
	EDT [75]	DF2K	38.45	0.9624	34.57	0.9258	32.52	0.9041	33.80	0.9425	39.93	0.9800
	HAT [75]	DF2K	38.63	0.9630	34.86	0.9274	32.62	0.9053	34.45	0.9466	40.26	0.9809
	SRFormer (ours)	DF2K	38.51	0.9627	34.44	0.9253	32.57	0.9046	34.09	0.9449	40.07	0.9802
	SRFormerV2 (ours) SRFormerV2+ (ours)	DF2K DF2K	38.63 38.68	0.9632 0.9633	34.90 34.93	0.9276 0.9278	32.64 32.67	0.9056 0.9059	34.59	0.9477 0.9485	40.40 40.51	0.9811 0.9813
	5Krormerv2+ (ours)		30.00			0.9278			34.77	0.9465	40.51	
	EDSR [10]	DIV2K	34.65	0.9280	30.52	0.8462	29.25	0.8093	28.80	0.8653	34.17	0.9476
	RCAN [17]	DIV2K	34.74	0.9299	30.65	0.8482	29.32	0.8111	29.09	0.8702	34.44	0.9499
	SAN [39]	DIV2K	34.75	0.9300	30.59	0.8476	29.33	0.8112	28.93	0.8671	34.30	0.9494
	IGNN [40]	DIV2K	34.72	0.9298	30.66	0.8484	29.31	0.8105	29.03	0.8696	34.39	0.9496
SR	HAN [35]	DIV2K	34.75	0.9299	30.67	0.8483	29.32	0.8110	29.10	0.8705	34.48	0.9500
×	NLSA [38]	DIV2K	34.85	0.9306	30.70	0.8485	29.34	0.8117	29.25	0.8726	34.57	0.9508
^	SwinIR [20]	DIV2K DIV2K	34.89	0.9312	30.77	0.8503	29.37 29.38	0.8124 0.8124	29.29 29.32	0.8744	34.74	0.9518 0.9517
	ELAN [22] SRFormer (ours)	DIV2K DIV2K	34.90 34.94	0.9313 0.9318	30.80 30.81	0.8504 0.8518	29.36 29.41	0.8124	29.52 29.52	0.8745 0.8786	34.73 34.78	0.9517 0.9524
												0.9324
	IPT [19]	ImageNet DF2K	34.81	- 0.9318	30.85	- 0.0524	29.38	- 0.0145	29.49	0.8826	- 25 12	0.9537
	SwinIR [20]	DF2K DF2K	34.97 34.97	0.9318	30.93 30.89	0.8534 0.8527	29.46 29.44	0.8145	29.75 29.72		35.12 35.13	0.9537
	EDT [75] HAT [75]	DF2K DF2K	35.07	0.9316	31.08	0.8555	29.44	0.8142 0.8167	30.23	0.8814 0.8896	35.13	0.9554
	SRFormer (ours)	DF2K DF2K	35.02	0.9323	30.94	0.8533	29.48	0.8156	30.23	0.8865	35.26	0.9532
	SRFormerV2 (ours)	DF2K DF2K	35.05	0.9323	31.10	0.8562	29.55	0.8176	30.46	0.8924	35.59	0.9557
	SRFormerV2+ (ours)	DF2K	35.14	0.9335	31.17	0.8569	29.59	0.8181	30.62	0.8941	35.73	0.9563
	EDSR [10]	DIV2K	32.46	0.8968	28.80	0.7876	27.71	0.7420	26.64	0.8033	31.02	0.9148
	RCAN [17]	DIV2K	32.63	0.9002	28.87	0.7889	27.77	0.7436	26.82	0.8087	31.22	0.9173
	SAN [39]	DIV2K	32.64	0.9003	28.92	0.7888	27.78	0.7436	26.79	0.8068	31.18	0.9169
	IGNN [40]	DIV2K	32.57	0.8998	28.85	0.7891	27.77	0.7434	26.84	0.8090	31.28	0.9182
SR	HAN [35]	DIV2K	32.64	0.9002	28.90	0.7890	27.80	0.7442	26.85	0.8094	31.42	0.9177
2,	NLSA [38]	DIV2K	32.59	0.9000	28.87	0.7891	27.78	0.7444	26.96	0.8109	31.27	0.9184
$\overset{\times}{4}$	SwinIR [20]	DIV2K	32.72	0.9021	28.94	0.7914	27.83	0.7459	27.07	0.8164	31.67	0.9226
	ELAN [22]	DIV2K	32.75	0.9022	28.96	0.7914	27.83	0.7459	27.13	0.8167	31.68	0.9226
	SRFormer (ours)	DIV2K	32.81	0.9029	29.01	0.7919	27.85	0.7472	27.20	0.8189	31.75	0.9237
	IPT [19]	ImageNet	32.64	-	29.01	-	27.82	-	27.26	-	-	-
	SwinIR [20]	DF2K	32.92	0.9044	29.09	0.7950	27.92	0.7489	27.45	0.8254	32.03	0.9260
	EDT [75]	DF2K	32.82	0.9031	29.09	0.7939	27.91	0.7483	27.46	0.8246	32.03	0.9254
	HAT [75]	DF2K	33.04	0.9056	29.23	0.7973	28.00	0.7517	27.97	0.8368	32.48	0.9292
	SRFormer (ours)	DF2K	32.93	0.9041	29.08	0.7953	27.94	0.7502	27.68	0.8311	32.21	0.9271
	SRFormerV2 (ours)	DF2K	33.06	0.9066	29.21	0.7978	27.98	0.7522	28.04	0.8391	32.52	0.9300
	SRFormerV2+ (ours)	DF2K	33.16	0.9069	29.28	0.7991	28.03	0.7530	28.17	0.8414	32.75	0.9313

5.3 Classical Image Super-Resolution

To evaluate the performance of SRFormer and SRFormerV2 on classical super-resolution task, we compare them with a series of state-of-the-art CNN-based and Transformer-based SR methods: RCAN [17], RDN [15], SAN [39], IGNN [40], HAN [35], NLSA [38], IPT [19], SwinIR [20], EDT [75], ELAN [22], and HAT [24].

Quantitative comparison. The quantitative comparison of the methods for classical image SR is shown in Table 5. For a fair comparison, the number of parameters and MACs of SRFormer are lower than SwinIR [20] (See Tab. 7 for details). It can be clearly seen that SRFormer achieves the

best performance on almost all five benchmark datasets for all scale factors. Since calculating self-attention within large windows can allow more information to be aggregated over a large area, our SRFormer performs much better on the high-resolution test set, such as Urban100 and Manga109. Especially, for the $\times 2$ SR training with DIV2K, our SRFormer achieves a 33.86dB PSNR score on the Urban100 dataset, which is 0.46dB higher than SwinIR but uses fewer parameters and computations. The above strongly supports that our SRFormer is effective and efficient. Through a series of enhancements to SRFormer described in Sec. 4, the upgraded SRFormerV2 achieves better results, surpassing

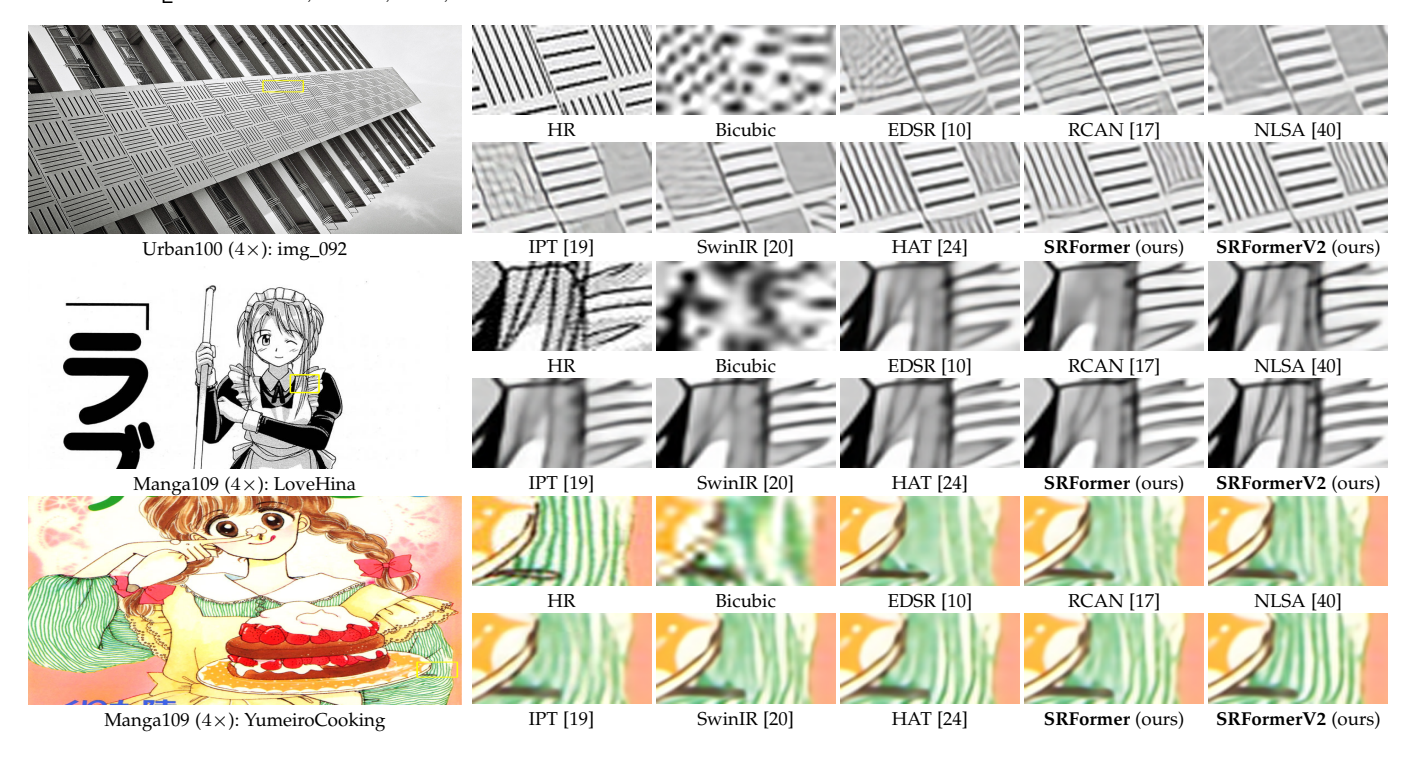


Fig. 6. Qualitative comparison with recent state-of-the-art classical image SR methods on the $\times 4$ SR task.

TABLE 6
Quantitative comparison of our SRFormer-light with recent state-of-the-art lightweight image SR methods on five benchmark datasets. The best performance among all the models is highlighted.

	Method	Training			MACs SET5 [68]		SET1	4 [69]	B100 [70]		Urban100 [26]		Manga109 [71]	
		Dataset			PSNR	SSIM	PSNR	SSIM	PSNR	SSIM	PSNR	SSIM	PSNR	SSIM
	EDSR-baseline [10]	DIV2K	1370K	316G	37.99	0.9604	33.57	0.9175	32.16	0.8994	31.98	0.9272	38.54	0.9769
	IMDN [76]	DIV2K	694K	158.8G	38.00	0.9605	33.63	0.9177	32.19	0.8996	32.17	0.9283	38.88	0.9774
	LAPAR-A [77]	DF2K	548K	171G	38.01	0.9605	33.62	0.9183	32.19	0.8999	32.10	0.9283	38.67	0.9772
SR	LatticeNet [78]	DIV2K	756K	169.5G	38.15	0.9610	33.78	0.9193	32.25	0.9005	32.43	0.9302	-	-
×2 5	ESRT [79]	DIV2K	751K	-	38.03	0.9600	33.75	0.9184	32.25	0.9001	32.58	0.9318	39.12	0.9774
×	SwinIR-light [20]	DIV2K	910K	244G	38.14	0.9611	33.86	0.9206	32.31	0.9012	32.76	0.9340	39.12	0.9783
	ELAN [22]	DIV2K	621K	203G	38.17	0.9611	33.94	0.9207	32.30	0.9012	32.76	0.9340	39.11	0.9782
	SRFormer-light	DIV2K	853K	236G	38.23	0.9613	33.94	0.9209	32.36	0.9019	32.91	0.9353	39.28	0.9785
	EDSR-baseline [10]	DIV2K	1555K	160G	34.37	0.9270	30.28	0.8417	29.09	0.8052	28.15	0.8527	33.45	0.9439
	IMDN [76]	DIV2K	703K	71.5G	34.36	0.9270	30.32	0.8417	29.09	0.8046	28.17	0.8519	33.61	0.9445
	LAPAR-A [77]	DF2K	594K	114G	34.36	0.9267	30.34	0.8421	29.11	0.8054	28.15	0.8523	33.51	0.9441
SR	LatticeNet [78]	DIV2K	765K	76.3G	34.53	0.9281	30.39	0.8424	29.15	0.8059	28.33	0.8538	-	-
33	ESRT [79]	DIV2K	751K	-	34.42	0.9268	30.43	0.8433	29.15	0.8063	28.46	0.8574	33.95	0.9455
×	SwinIR-light [20]	DIV2K	918K	111G	34.62	0.9289	30.54	0.8463	29.20	0.8082	28.66	0.8624	33.98	0.9478
	ELAN [22]	DIV2K	629K	90.1G	34.61	0.9288	30.55	0.8463	29.21	0.8081	28.69	0.8624	34.00	0.9478
	SRFormer-light	DIV2K	861K	105G	34.67	0.9296	30.57	0.8469	29.26	0.8099	28.81	0.8655	34.19	0.9489
	EDSR-baseline [10]	DIV2K	1518K	114G	32.09	0.8938	28.58	0.7813	27.57	0.7357	26.04	0.7849	30.35	0.9067
	IMDN [76]	DIV2K	715K	40.9G	32.21	0.8948	28.58	0.7811	27.56	0.7353	26.04	0.7838	30.45	0.9075
	LAPAR-A [77]	DF2K	659K	94G	32.15	0.8944	28.61	0.7818	27.61	0.7366	26.14	0.7871	30.42	0.9074
SR	LatticeNet [78]	DIV2K	777K	43.6G	32.30	0.8962	28.68	0.7830	27.62	0.7367	26.25	0.7873	-	-
4	ESRT [79]	DIV2K	751K	-	32.19	0.8947	28.69	0.7833	27.69	0.7379	26.39	0.7962	30.75	0.9100
×	SwinIR-light [20]	DIV2K	930K	63.6G	32.44	0.8976	28.77	0.7858	27.69	0.7406	26.47	0.7980	30.92	0.9151
	ELAN [22]	DIV2K	640K	54.1G	32.43	0.8975	28.78	0.7858	27.69	0.7406	26.54	0.7982	30.92	0.9150
	SRFormer-light	DIV2K	873K	62.8G	32.51	0.8988	28.82	0.7872	27.73	0.7422	26.67	0.8032	31.17	0.9165

the previous state-of-the-art model HAT.

Qualitative comparison. We show qualitative comparisons of our SRFormer and our advanced SRFormerV2 with recent state-of-the-art methods in Fig. 6. From each example of Fig. 6, one can clearly observe that SRFormer can restore crisper and detailed textures and edges. In contrast, the

previous models restore blurred or low-quality textures. The qualitative comparison shows that our SRFormer can restore better high-resolution images from the low-resolution ones. Through a series of enhancements described in Sec. 4, SRFormerV2 further enhances image clarity and achieves much better results than all of the previous works.

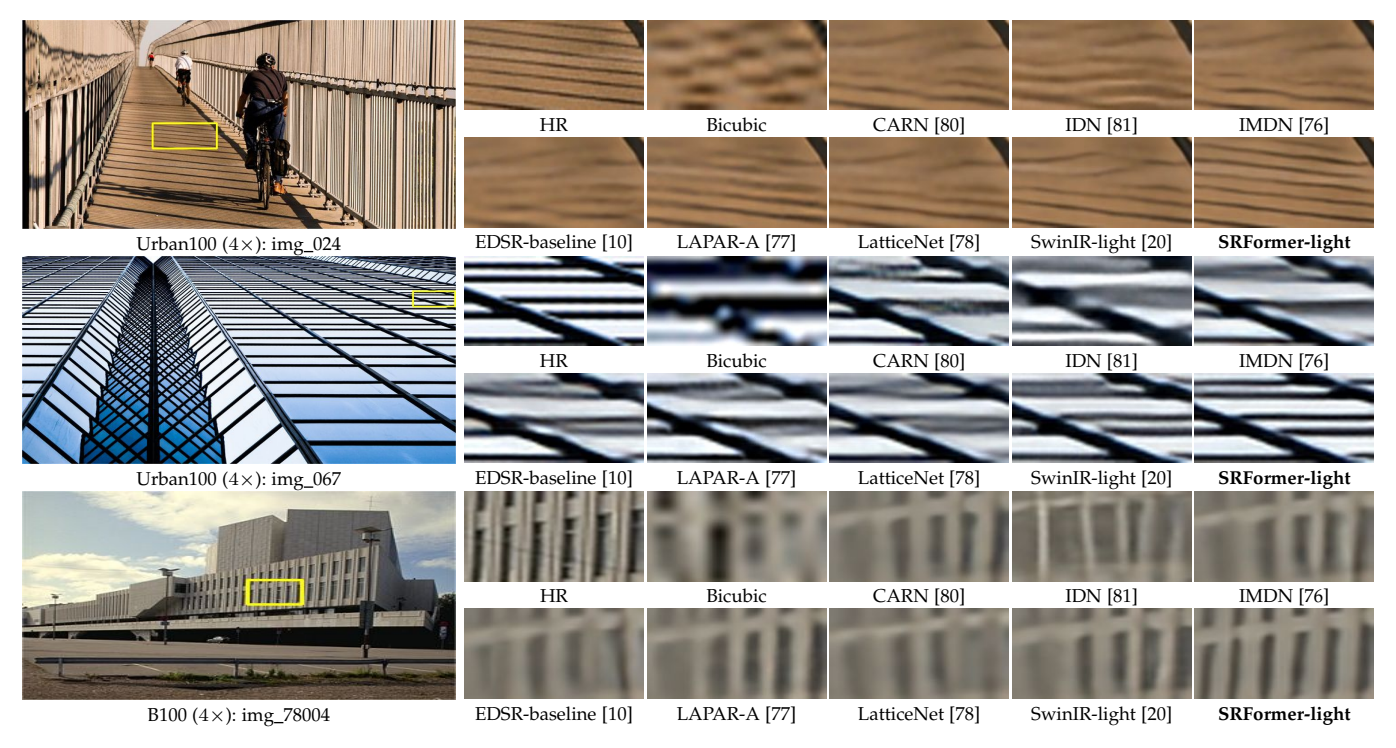


Fig. 7. Qualitative comparison of our SRFormerV2-light with recent state-of-the-art **lightweight image SR** methods for the $\times 4$ SR task. For each example, our SRFormerV2-light can restore the structures and details better than other methods.

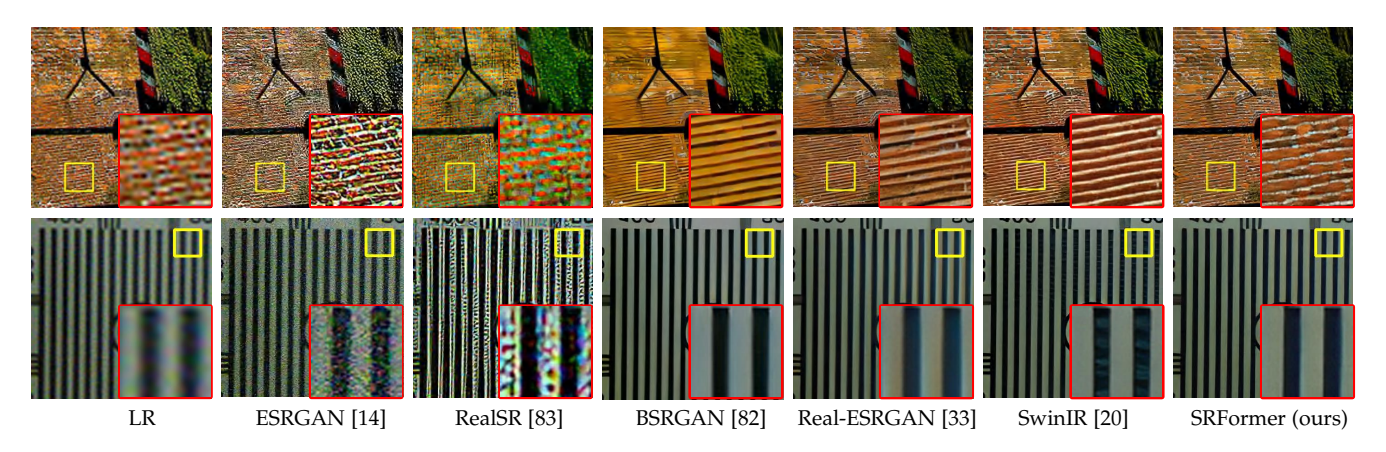


Fig. 8. Qualitative comparisons with recent state-of-the-art methods on the $\times 4$ real-world image SR task. Our method can better restore the edges and textures compared to other methods.

5.4 Lightweight Image Super-Resolution

To demonstrate our model's scalability and further proof of SRFormer's efficiency and effectiveness, we train SRFormer-light and compare it with a list of state-of-the-art lightweight SR methods: EDSR-baseline [10], CARN [80], IMDN [76], LAPAR-A [77], LatticeNet [78], ESRT [79], SwinIR-light [20], and ELAN [22].

Quantitative comparison. The quantitative comparisons of lightweight image SR models are shown in Tab. 6. Following previous works [78], [80], we report the MACs by upscaling a low-resolution image to 1280×720 resolution on all scales. We can see that our SRFormer-light achieves the best performance on all five benchmark datasets for all scale factors. Our model outperforms SwinIR-light [20] by up to 0.20 dB PSNR scores on the Urban100 dataset and 0.25 dB PSNR scores on the Manga109 dataset with even fewer

parameters and MACs. The results indicate that despite the simplicity, our permuted self-attention is a more effective way to encode spatial information.

Qualitative comparison. We compare our SRFormer with state-of-the-art lightweight image SR models for qualitative comparisons in Fig. 7. Notably, for all examples in Fig. 7, SRFormer-light is the only model that can restore the main structures with less blurring and artifacts. This strongly demonstrates that the light version of SRFormer also performs better for restoring edges and textures compared to other methods.

5.5 Real-World Image Super-Resolution

To test the performance of SRFormer under a broader range of image degradation scenarios, we follow SwinIR [20] to retrain our SRFormer by using the same degradation model as BSRGAN [82] and show results in Fig. 8. SRFormer still produces more realistic and visually pleasing textures without artifacts when faced with real-world images, which demonstrates the robustness of our method.

5.6 Model Size Comparison

While achieving the state-of-the-art performance, our SR-Former is also efficient. In Tab. 7, we compare the parameters and MACs of our SRFormer with recent state-of-the-art models. Following previous works [78], [80], we report the MACs by upscaling a low-resolution image to 1280×720 resolution. One can clearly find that the performance of our SRFormer exceeds SwinIR [20] with fewer parameters and MACs.

In our SRFormerV2, we explore the scaling capabilities of SRFormer. Compared with HAT, our SRFormerV2 has similar parameters and computational load but greatly exceeds HAT in performance. We also train a smaller scaling model, named SRFormerV2-S, which follows the advanced operations in Fig. 5 but has 180 channels. It requires much fewer computational resources than HAT but also performs better than it as shown in Tab. 7. To further verify the effectiveness of PSA, we also replace the window attention in HAT with PSA using a 36×36 attention window size, which can also enhance the performance of HAT on both the Urban100 and Manga109 datasets.

TABLE 7
Model size comparisons (×2 SR). We report PSNR on Urban100 and Manga109. All models are trained on the DF2K (DIV2K [10] + Flickr2K [72]) training set.

Method	Params	MACs	Urban100	Manga109
SwinIR [20]	11.80M	2.9T	33.81	39.92
SRFormer	10.52M	2.7T	34.09	40.07
HAT [24]	20.6M	5.9T	34.45	40.26
HAT + our PSA	18.9M	5.6T	34.57	40.32
SRFormerV2-S	15.0M	4.8T	34.56	40.35
SRFormerV2	21.9M	6.1T	34.59	40.40

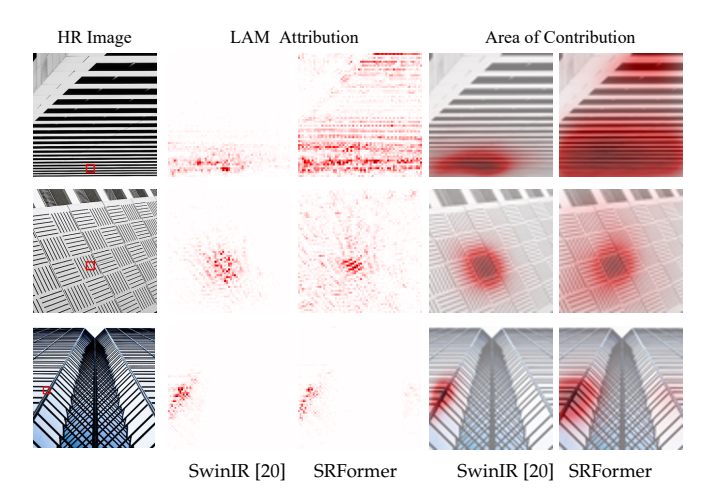


Fig. 9. LAM results of SwinIR [20] and SRFormer on multiple challenging examples. We can see that SRFormer can perform SR reconstruction based on a particularly wide range of pixels.

5.7 LAM Comparison

To observe the range of utilized pixels for super-resolution (SR) reconstruction of our PSA, we compare SRFormer with SwinIR using LAM [84] on multiple challenging examples. Given a specified region in the SR image, LAM analyzes the contributions of each pixel in the input image to reconstruct this region. The results are shown in Fig. 9. From the first two examples, we can see that SRFormer performs reconstruction based on almost all the pixels of input because similar textures are repeated in the whole image. For the last example, a more amazing phenomenon can be observed that SRFormer can span long distances and use the pixels on the right side for the reconstruction of the left region since the image is left-right symmetrical. This proves that the SRFormer can extract the available features from almost the entire image for inference SR images in this case. Experimental results indicate that SRFormer infers SR images with a significantly wider range of pixels than SwinIR [20].

6 CONCLUSION

In this paper, we propose PSA, an efficient self-attention mechanism that can efficiently build pairwise correlations within large windows. Based on our PSA, we design a simple yet effective Transformer-based model for single image super-resolution, called SRFormer. Due to the extremely large attention window and high-frequency information enhancement, SRFormer performs excellently on classical, lightweight, and real-world SR tasks. In order to further investigate the potential of PSA, we further conduct scaling research and propose SRFormerV2, achieving new state-of-the-art performance. We hope our permuted self-attention can be a paradigm of large window self-attention and serve as a useful tool for future research in super-resolution model design.

REFERENCES

- [1] Y. Zhou, Z. Li, C.-L. Guo, S. Bai, M.-M. Cheng, and Q. Hou, "Srformer: Permuted self-attention for single image super-resolution," in *Int. Conf. Comput. Vis.*, 2023.
- [2] Y. Jo, S. W. Oh, J. Kang, and S. J. Kim, "Deep video superresolution network using dynamic upsampling filters without explicit motion compensation," in *IEEE Conf. Comput. Vis. Pattern Recog.*, 2018.
- [3] X. Wang, K. C. Chan, K. Yu, C. Dong, and C. Change Loy, "Edvr: Video restoration with enhanced deformable convolutional networks," in *IEEE Conf. Comput. Vis. Pattern Recog. Worksh.*, 2019.
- [4] S. Anwar, S. Khan, and N. Barnes, "A deep journey into superresolution: A survey," ACM Computing Surveys, 2020.
- [5] C. Dong, C. C. Loy, K. He, and X. Tang, "Learning a deep convolutional network for image super-resolution," in Eur. Conf. Comput. Vis., 2014.
- [6] J. Kim, J. K. Lee, and K. M. Lee, "Accurate image super-resolution using very deep convolutional networks," in *IEEE Conf. Comput. Vis. Pattern Recog.*, 2016.
- [7] K. Zhang, W. Zuo, and L. Zhang, "Learning a single convolutional super-resolution network for multiple degradations," in *IEEE Conf. Comput. Vis. Pattern Recog.*, 2018.
- [8] C. Ledig, L. Theis, F. Huszár, J. Caballero, A. Cunningham, A. Acosta, A. Aitken, A. Tejani, J. Totz, Z. Wang et al., "Photorealistic single image super-resolution using a generative adversarial network," in *IEEE Conf. Comput. Vis. Pattern Recog.*, 2017.
- [9] W. Shi, J. Caballero, F. Huszár, J. Totz, A. P. Aitken, R. Bishop, D. Rueckert, and Z. Wang, "Real-time single image and video super-resolution using an efficient sub-pixel convolutional neural network," in *IEEE Conf. Comput. Vis. Pattern Recog.*, 2016.

- [10] B. Lim, S. Son, H. Kim, S. Nah, and K. Mu Lee, "Enhanced deep residual networks for single image super-resolution," in *IEEE Conf. Comput. Vis. Pattern Recog. Worksh.*, 2017.
- [11] Y. Tai, J. Yang, and X. Liu, "Image super-resolution via deep recursive residual network," in *IEEE Conf. Comput. Vis. Pattern Recog.*, 2017.
- [12] K. Zhang, Y. Li, W. Zuo, L. Zhang, L. Van Gool, and R. Timofte, "Plug-and-play image restoration with deep denoiser prior," *IEEE Trans. Pattern Anal. Mach. Intell.*, 2021.
- [13] J. Li, F. Fang, K. Mei, and G. Zhang, "Multi-scale residual network for image super-resolution," in Eur. Conf. Comput. Vis., 2018.
- [14] X. Wang, K. Yu, S. Wu, J. Gu, Y. Liu, C. Dong, Y. Qiao, and C. Change Loy, "Esrgan: Enhanced super-resolution generative adversarial networks," in Eur. Conf. Comput. Vis. Worksh., 2018.
- [15] Y. Zhang, Y. Tian, Y. Kong, B. Zhong, and Y. Fu, "Residual dense network for image super-resolution," in *IEEE Conf. Comput. Vis. Pattern Recog.*, 2018.
- [16] T. Tong, G. Li, X. Liu, and Q. Gao, "Image super-resolution using dense skip connections," in *Int. Conf. Comput. Vis.*, 2017.
- [17] Y. Zhang, K. Li, K. Li, L. Wang, B. Zhong, and Y. Fu, "Image superresolution using very deep residual channel attention networks," in *Eur. Conf. Comput. Vis.*, 2018.
- [18] Y. Yang and Y. Qi, "Image super-resolution via channel attention and spatial graph convolutional network," *Pattern Recognition*, 2021.
- [19] H. Chen, Y. Wang, T. Guo, C. Xu, Y. Deng, Z. Liu, S. Ma, C. Xu, C. Xu, and W. Gao, "Pre-trained image processing transformer," in *IEEE Conf. Comput. Vis. Pattern Recog.*, 2021.
- [20] J. Liang, J. Cao, G. Sun, K. Zhang, L. Van Gool, and R. Timofte, "Swinir: Image restoration using swin transformer," in *Int. Conf. Comput. Vis. Worksh.*, 2021.
- [21] D. Zhang, F. Huang, S. Liu, X. Wang, and Z. Jin, "Swinfir: Revisiting the swinir with fast fourier convolution and improved training for image super-resolution," *arXiv*:2208.11247, 2022.
- [22] X. Zhang, H. Zeng, S. Guo, and L. Zhang, "Efficient long-range attention network for image super-resolution," arXiv:2203.06697, 2022.
- [23] Z. Liu, Y. Lin, Y. Cao, H. Hu, Y. Wei, Z. Zhang, S. Lin, and B. Guo, "Swin transformer: Hierarchical vision transformer using shifted windows," in *Int. Conf. Comput. Vis.*, 2021.
- [24] X. Chen, X. Wang, J. Zhou, and C. Dong, "Activating more pixels in image super-resolution transformer," arXiv:2205.04437, 2022.
- [25] H. Touvron, M. Cord, A. Sablayrolles, G. Synnaeve, and H. Jégou, "Going deeper with image transformers," in *Int. Conf. Comput. Vis.*, 2021.
- [26] J.-B. Huang, A. Singh, and N. Ahuja, "Single image superresolution from transformed self-exemplars," in *IEEE Conf. Com*put. Vis. Pattern Recog., 2015.
- [27] J. Kim, J. K. Lee, and K. M. Lee, "Deeply-recursive convolutional network for image super-resolution," in *IEEE Conf. Comput. Vis. Pattern Recog.*, 2016.
- [28] Y. Tai, J. Yang, X. Liu, and C. Xu, "Memnet: A persistent memory network for image restoration," in *Int. Conf. Comput. Vis.*, 2017.
- [29] C. Dong, C. C. Loy, and X. Tang, "Accelerating the superresolution convolutional neural network," in Eur. Conf. Comput. Vis., 2016.
- [30] W.-S. Lai, J.-B. Huang, N. Ahuja, and M.-H. Yang, "Deep laplacian pyramid networks for fast and accurate super-resolution," in *IEEE Conf. Comput. Vis. Pattern Recog.*, 2017.
- [31] M. Haris, G. Shakhnarovich, and N. Ukita, "Deep back-projection networks for super-resolution," in *IEEE Conf. Comput. Vis. Pattern Recog.*, 2018.
- [32] W. Zhang, Y. Liu, C. Dong, and Y. Qiao, "Ranksrgan: Generative adversarial networks with ranker for image super-resolution," in Int. Conf. Comput. Vis., 2019.
- [33] X. Wang, L. Xie, C. Dong, and Y. Shan, "Real-esrgan: Training real-world blind super-resolution with pure synthetic data," in *Int. Conf. Comput. Vis.*, 2021.
- [34] I. J. Goodfellow, J. Pouget-Abadie, M. Mirza, B. Xu, D. Warde-Farley, S. Ozair, A. Courville, and Y. Bengio, "Generative adversarial networks," *arXiv:1406.2661*, 2014.
- [35] B. Niu, W. Wen, W. Ren, X. Zhang, L. Yang, S. Wang, K. Zhang, X. Cao, and H. Shen, "Single image super-resolution via a holistic attention network," in Eur. Conf. Comput. Vis., 2020.
- [36] X. Wang, R. Girshick, A. Gupta, and K. He, "Non-local neural networks," in *IEEE Conf. Comput. Vis. Pattern Recog.*, 2018.

- [37] Y. Mei, Y. Fan, Y. Zhou, L. Huang, T. S. Huang, and H. Shi, "Image super-resolution with cross-scale non-local attention and exhaustive self-exemplars mining," in *IEEE Conf. Comput. Vis. Pattern Recog.*, 2020.
- [38] Y. Mei, Y. Fan, and Y. Zhou, "Image super-resolution with non-local sparse attention," in *IEEE Conf. Comput. Vis. Pattern Recog.*, 2021.
- [39] T. Dai, J. Cai, Y. Zhang, S.-T. Xia, and L. Zhang, "Second-order attention network for single image super-resolution," in *IEEE Conf. Comput. Vis. Pattern Recog.*, 2019.
- [40] S. Zhou, J. Zhang, W. Zuo, and C. C. Loy, "Cross-scale internal graph neural network for image super-resolution," in Adv. Neural Inform. Process. Syst., 2020.
- [41] A. Dosovitskiy, L. Beyer, A. Kolesnikov, D. Weissenborn, X. Zhai, T. Unterthiner, M. Dehghani, M. Minderer, G. Heigold, S. Gelly et al., "An image is worth 16x16 words: Transformers for image recognition at scale," in *Int. Conf. Learn. Represent.*, 2020.
- [42] H. Touvron, M. Cord, M. Douze, F. Massa, A. Sablayrolles, and H. Jégou, "Training data-efficient image transformers & distillation through attention," arXiv:2012.12877, 2020.
- [43] L. Yuan, Y. Chen, T. Wang, W. Yu, Y. Shi, Z.-H. Jiang, F. E. Tay, J. Feng, and S. Yan, "Tokens-to-token vit: Training vision transformers from scratch on imagenet," in *Int. Conf. Comput. Vis.*, 2021.
- [44] W. Wang, E. Xie, X. Li, D.-P. Fan, K. Song, D. Liang, T. Lu, P. Luo, and L. Shao, "Pyramid vision transformer: A versatile backbone for dense prediction without convolutions," in *Int. Conf. Comput. Vis.*, 2021.
- [45] L. Yuan, Q. Hou, Z. Jiang, J. Feng, and S. Yan, "Volo: Vision outlooker for visual recognition," *IEEE Trans. Pattern Anal. Mach. Intell.*, 2022.
- [46] N. Carion, F. Massa, G. Synnaeve, N. Usunier, A. Kirillov, and S. Zagoruyko, "End-to-end object detection with transformers," in *Eur. Conf. Comput. Vis.*, 2020.
- [47] Z. Sun, S. Cao, Y. Yang, and K. M. Kitani, "Rethinking transformer-based set prediction for object detection," in *Int. Conf. Comput. Vis.*, 2021.
- [48] Y. Fang, B. Liao, X. Wang, J. Fang, J. Qi, R. Wu, J. Niu, and W. Liu, "You only look at one sequence: Rethinking transformer in vision through object detection," in Adv. Neural Inform. Process. Syst., 2021
- [49] E. Xie, W. Wang, Z. Yu, A. Anandkumar, J. M. Alvarez, and P. Luo, "Segformer: Simple and efficient design for semantic segmentation with transformers," in *Adv. Neural Inform. Process. Syst.*, 2021.
- [50] S. Zheng, J. Lu, H. Zhao, X. Zhu, Z. Luo, Y. Wang, Y. Fu, J. Feng, T. Xiang, P. H. Torr et al., "Rethinking semantic segmentation from a sequence-to-sequence perspective with transformers," in *IEEE Conf. Comput. Vis. Pattern Recog.*, 2021.
- [51] R. Strudel, R. Garcia, I. Laptev, and C. Schmid, "Segmenter: Transformer for semantic segmentation," in *Int. Conf. Comput. Vis.*, 2021.
- [52] S. W. Zamir, A. Arora, S. Khan, M. Hayat, F. S. Khan, and M.-H. Yang, "Restormer: Efficient transformer for high-resolution image restoration," in *IEEE Conf. Comput. Vis. Pattern Recog.*, 2022.
- [53] Y. Jiang, S. Chang, and Z. Wang, "Transgan: Two transformers can make one strong gan," arXiv:2102.07074, 2021.
- [54] K. Lee, H. Chang, L. Jiang, H. Zhang, Z. Tu, and C. Liu, "Vitgan: Training gans with vision transformers," arXiv:2107.04589, 2021.
- [55] B. Zhang, S. Gu, B. Zhang, J. Bao, D. Chen, F. Wen, Y. Wang, and B. Guo, "Styleswin: Transformer-based gan for high-resolution image generation," in *IEEE Conf. Comput. Vis. Pattern Recog.*, 2022.
- [56] Y. Deng, F. Tang, W. Dong, C. Ma, X. Pan, L. Wang, and C. Xu, "Stytr2: Image style transfer with transformers," in *IEEE Conf. Comput. Vis. Pattern Recog.*, 2022.
- [57] L. Lu, R. Wu, H. Lin, J. Lu, and J. Jia, "Video frame interpolation with transformer," in IEEE Conf. Comput. Vis. Pattern Recog., 2022.
- [58] R. Liu, H. Deng, Y. Huang, X. Shi, L. Lu, W. Sun, X. Wang, J. Dai, and H. Li, "Fuseformer: Fusing fine-grained information in transformers for video inpainting," in *Int. Conf. Comput. Vis.*, 2021.
- [59] J. Ren, Q. Zheng, Y. Zhao, X. Xu, and C. Li, "Dlformer: Discrete latent transformer for video inpainting," in *IEEE Conf. Comput. Vis. Pattern Recog.*, 2022.
- [60] C. Liu, H. Yang, J. Fu, and X. Qian, "Learning trajectory-aware transformer for video super-resolution," in *IEEE Conf. Comput. Vis. Pattern Recog.*, 2022.

- [61] Z. Geng, L. Liang, T. Ding, and I. Zharkov, "Rstt: Real-time spatial temporal transformer for space-time video super-resolution," in *IEEE Conf. Comput. Vis. Pattern Recog.*, 2022.
- [62] Z. Wang, X. Cun, J. Bao, W. Zhou, J. Liu, and H. Li, "Uformer: A general u-shaped transformer for image restoration," in *IEEE Conf. Comput. Vis. Pattern Recog.*, 2022.
- [63] C.-L. Guo, Q. Yan, S. Anwar, R. Cong, W. Ren, and C. Li, "Image dehazing transformer with transmission-aware 3d position embedding," in *IEEE Conf. Comput. Vis. Pattern Recog.*, 2022.
- [64] N. Park and S. Kim, "How do vision transformers work?" in Int. Conf. Learn. Represent., 2022.
- [65] P. Wang, W. Zheng, T. Chen, and Z. Wang, "Anti-oversmoothing in deep vision transformers via the fourier domain analysis: From theory to practice," *arXiv:2203.05962*, 2022.
- [66] Z. Wang, A. C. Bovik, H. R. Sheikh, and E. P. Simoncelli, "Image quality assessment: from error visibility to structural similarity," *IEEE transactions on image processing*, 2004.
- [67] F. Kong, M. Li, S. Liu, D. Liu, J. He, Y. Bai, F. Chen, and L. Fu, "Residual local feature network for efficient super-resolution," in *Proceedings of the IEEE/CVF Conference on Computer Vision and Pattern Recognition*, 2022, pp. 766–776.
- [68] M. Bevilacqua, A. Roumy, C. Guillemot, and M. L. Alberi-Morel, "Low-complexity single-image super-resolution based on nonnegative neighbor embedding," in BMVC, 2012.
- [69] R. Zeyde, M. Elad, and M. Protter, "On single image scale-up using sparse-representations," in Curves and Surfaces, 2010.
- [70] D. Martin, C. Fowlkes, D. Tal, and J. Malik, "A database of human segmented natural images and its application to evaluating segmentation algorithms and measuring ecological statistics," in *Int. Conf. Comput. Vis.*, 2001.
- [71] Y. Matsui, K. Ito, Y. Aramaki, A. Fujimoto, T. Ogawa, T. Yamasaki, and K. Aizawa, "Sketch-based manga retrieval using manga109 dataset," Multimedia Tools and Applications, 2017.
- [72] R. Timofte, E. Agustsson, L. Van Gool, M.-H. Yang, and L. Zhang, "Ntire 2017 challenge on single image super-resolution: Methods and results," in *IEEE Conf. Comput. Vis. Pattern Recog. Worksh.*, 2017.
- [73] X. Wang, K. Yu, C. Dong, and C. C. Loy, "Recovering realistic texture in image super-resolution by deep spatial feature transform," in *IEEE Conf. Comput. Vis. Pattern Recog.*, 2018.
- [74] D. P. Kingma and J. Ba, "Adam: A method for stochastic optimization," arXiv:1412.6980, 2014.
- [75] W. Li, X. Lu, J. Lu, X. Zhang, and J. Jia, "On efficient transformer and image pre-training for low-level vision," arXiv:2112.10175, 2022.
- [76] Z. Hui, X. Gao, Y. Yang, and X. Wang, "Lightweight image superresolution with information multi-distillation network," in ACM Int. Conf. Multimedia, 2019.
- [77] W. Li, K. Zhou, L. Qi, N. Jiang, J. Lu, and J. Jia, "Lapar: Linearly-assembled pixel-adaptive regression network for single image super-resolution and beyond," in Adv. Neural Inform. Process. Syst., 2020.
- [78] X. Luo, Y. Xie, Y. Zhang, Y. Qu, C. Li, and Y. Fu, "Latticenet: Towards lightweight image super-resolution with lattice block," in *Eur. Conf. Comput. Vis.*, 2020.
- [79] Z. Lu, H. Liu, J. Li, and L. Zhang, "Efficient transformer for single image super-resolution," arXiv:2108.11084, 2021.
- [80] N. Ahn, B. Kang, and K.-A. Sohn, "Fast, accurate, and lightweight super-resolution with cascading residual network," in Eur. Conf. Comput. Vis., 2018.
- [81] Z. Hui, X. Wang, and X. Gao, "Fast and accurate single image super-resolution via information distillation network," in IEEE Conf. Comput. Vis. Pattern Recog., 2018.
- [82] K. Zhang, J. Liang, L. V. Gool, and R. Timofte, "Designing a practical degradation model for deep blind image super-resolution," in Int. Conf. Comput. Vis., 2021.
- [83] X. Ji, Y. Cao, Y. Tai, C. Wang, J. Li, and F. Huang, "Real-world super-resolution via kernel estimation and noise injection," in IEEE Conf. Comput. Vis. Pattern Recog. Worksh., 2020.
- [84] J. Gu and C. Dong, "Interpreting super-resolution networks with local attribution maps," in *IEEE Conf. Comput. Vis. Pattern Recog.*, 2021.



Yupeng Zhou is currently working toward the PhD degree in the College of Computer Science, Nankai University, under the supervision of Prof. Qibin Hou. He received his bachelor's degree from Shandong University in 2022. His research interests include computer vision and deep learning, with a particular focus on image/video restoration and generation.



Zhen Li is currently working toward the PhD degree in the College of Computer Science, Nankai University, under the co-supervision of Prof. Ming-Ming Cheng and Prof. Xiu-Li Shao. He received his MS degree from Sichuan University in 2019. His research interests include computer vision and deep learning, particularly focusing on image/video restoration and enhancement, generation and editing, etc.



Chun-Le Guo received the Ph.D.degree from Tianjin University, China, under the supervision of Prof. ji-Chang Guo. He was a Visiting Ph.D. Student with the School of Electronic Engineering and Computer Science, Queen Mary University of London (QMUL), U.K. He was a Research Associate with the Department of Computer Science, City University of Hong Kong (CityU of HK). He was a Postdoctoral Researcher with Prof. Ming-Ming Cheng at Nankai University. He is currently an Associate Professor with Nankai

University. His research interests include image processing, computer vision, and deep learning.



Li Liu received her Ph.D. degree in information and communication engineering from the National University of Defence Technology, China, in 2012. She joined the faculty at the National University of Defense Technology in 2012. During her PhD study, she spent more than two years as a Visiting Student at the University of Waterloo, Canada, from 2008 to 2010. From 2015 to 2016, she spent ten months visiting the Multimedia Laboratory at the Chinese University of Hong Kong. From 2016 to 2018, she was

a senior researcher of the CMVS at the University of Oulu, Finland. Dr. Liu was co-chair of nine International Workshops at several major venues, including CVPR, ICCV, and ECCV; she served as the leading guest editor of the special issues for IEEE TPAMI and IJCV. She also served as Area Chair for ICME 2020, 2021, 2022, and ACCV 2020, 2022. She currently serves as Associate Editor for IEEE Transactions on Circuits and Systems for Pattern Video Technology, IEEE Transactions on Geoscience and Remote Sensing, and Pattern Recognition. Her current research interests include computer vision, pattern recognition, and machine learning. Her papers currently have over 14000 citations in Google Scholar. She is a senior member of the IEEE.



Ming-Ming Cheng received his PhD degree from Tsinghua University in 2012. Then he did 2 years research fellow, with Prof. Philip Torr in Oxford. He is now a professor at Nankai University, leading the Media Computing Lab. His research interests include computer graphics, computer vision, and image processing. He received research awards including National Science Fund for Distinguished Young Scholars and ACM China Rising Star Award. He is on the editorial boards of IEEE TPAMI and IEEE TIP.



Qibin Hou received his Ph.D. degree from the School of Computer Science, Nankai University. Then, he worked at the National University of Singapore as a research fellow. Now, he is an associate professor at School of Computer Science, Nankai University. He has published more than 30 papers on top conferences/journals, including T-PAMI, CVPR, ICCV, NeurIPS, etc. His research interests include deep learning and computer vision.